

## Scalable and model-free detection of spatial patterns and colocalization

Qi Liu<sup>1,2\*</sup>, Chih-Yuan Hsu<sup>1,2</sup>, Yu Shyr<sup>1,2\*</sup>

4 <sup>1</sup>Department of Biostatistics, Vanderbilt University Medical Center, Nashville, TN 37232, USA

5 <sup>2</sup>Center for Quantitative Sciences, Vanderbilt University Medical Center, Nashville, TN 37232, USA

6 \*Corresponding author: [qi.liu@vanderbilt.edu](mailto:qi.liu@vanderbilt.edu); [yu.shyr@vanderbilt.edu](mailto:yu.shyr@vanderbilt.edu)

## 7 Running Title: SpaGene - spatially variable genes detection

8

9

10

11

12

13

14

15

16

17

18

10

20 **ABSTRACT**

21 The expeditious growth in spatial omics technologies enable profiling genome-wide molecular events at  
22 molecular and single-cell resolution, highlighting a need for fast and reliable methods to characterize spatial  
23 patterns. We developed SpaGene, a model-free method to discover any spatial patterns rapidly in large  
24 scale spatial omics studies. Analyzing simulation and a variety of spatial resolved transcriptomics data  
25 demonstrated that SpaGene is more powerful and scalable than existing methods. Spatial expression  
26 patterns by SpaGene reconstructed unobserved tissue structures. SpaGene also successfully discovered  
27 ligand-receptor interactions through their colocalization.

28

29

30

31

32

33

34

35

36

37

38

## 39 INTRODUCTION

40 Spatial omics technologies map out organizational structures of cells along with their genomics,  
41 transcriptomics, proteomics and epigenomics profiles, providing powerful tools for deciphering  
42 mechanisms of functional and spatial arrangements in normal development and disease pathology (Larsson  
43 et al. 2021; Longo et al. 2021; Marx 2021; Deng et al. 2022; Dhainaut et al. 2022; Ratz et al. 2022; Zhao et  
44 al. 2022). The collection of available approaches provides a wide spectrum of throughput and spatial  
45 resolution. Imaging-based approaches generally target pre-selected RNA or proteins at molecular and single  
46 cell resolution, while sequencing-based approaches allow genome-wide profiling with limited spatial  
47 resolution (Lewis et al. 2021; Zhuang 2021). Recent advances in those approaches move the field rapidly  
48 into the direction achieving both high throughput and spatial resolution, presenting a significant  
49 computational challenge for scalable and robust methods to derive biological insights in the spatial context  
50 (Atta and Fan 2021).

51 One essential step in spatial omics analysis is to characterize spatial expression patterns and colocalization.  
52 Several methods have been developed to identify spatially variable genes (Edsgard et al. 2018; Svensson et  
53 al. 2018; Sun et al. 2020a; Anderson and Lundeberg 2021; Miller et al. 2021; Zhu et al. 2021). Trendsseek  
54 uses permutation test to detect significant dependency between the spatial distribution of points and their  
55 expression levels based on marked point processes (Edsgard et al. 2018). Sepal ranks spatially variable  
56 genes by the diffusion time with the rational that genes with spatial patterns require more time to reach a  
57 homogenous state than those with random spatial distributions (Anderson and Lundeberg 2021). SpatialDE  
58 and SPARK both utilize Gaussian process regression as the underlying data generative model for spatial  
59 covariance structures. SpatialDE decomposes expression variability into spatial variance and noise, and  
60 estimates statistical significance by comparing the likelihoods with and without a spatial component  
61 (Svensson et al. 2018). SPARK extends SpatialDE via generalized linear spatial error models, with the  
62 ability to directly model raw counts and adjust for covariates (Sun et al. 2020a). SPARK-X examines the  
63 similarity of expression covariance matrix and distance covariance matrix and tests whether they are more

64 similar than expected by chance (Zhu et al. 2021). The statistical power of such methods highly depends  
65 on spatial covariance models, i.e, how well they match true underlying expression patterns. Although  
66 multiple kernels, including Gaussian, linear and periodic kernels with different smoothness parameters, are  
67 considered to ensure identification of various spatial patterns, statistical power will be compromised  
68 substantially for identifying spatial patterns poorly modelled by those predefined kernel functions.  
69 Furthermore, spatial covariance models are built upon cellular distances, which would confound true  
70 expression variances with those driven by variances in cellular densities. To take non-uniform cellular  
71 densities into consideration, MERINGUE calculates spatial autocorrelation and cross-correlation based on  
72 spatial neighborhood graphs to identify spatially variable genes and gene interactions (Miller et al. 2021).  
73 Above all, even equipped with computationally efficient algorithms, it would still take days to months for  
74 most methods to analyze large-scale spatial data with genome-wide profiling in tens of thousands of  
75 locations (Zhu et al. 2021), resulting in a high demand for scalable and robust methods for characterizing  
76 spatial expression patterns.

77 Here we developed SpaGene, a scalable and model-free method for detecting spatial patterns. SpaGene is  
78 built upon a simple intuition that spatially variable genes have uneven spatial distribution, meaning that  
79 cells/spots with high expression tend to be more spatially connected than random. SpaGene is one of the  
80 most computationally efficient methods, which only takes seconds to minutes for analyzing large-scale  
81 spatial omics data. Independent of spatial covariance models and cellular densities, SpaGene demonstrated  
82 the power to identify any spatial patterns in the simulation and a variety of spatial transcriptomics datasets.  
83 Spatial expression patterns by SpaGene reconstructed unobserved tissue structures. Extended to identify  
84 spatial colocalization, SpaGene successfully discovered cell-cell communications mediated by ligand-  
85 receptor interactions.

## 86 RESULTS

### 87 Simulation

88 A schematic diagram of SpaGene is shown in Fig. 1A, with details in the Methods section. We first applied  
89 SpaGene on two simulation datasets. One simulation was generated from negative binomial distributions  
90 following SPARK-X (Zhu et al. 2021), the other was sampled from real data following Trendsseek  
91 (Edsgard et al. 2018). Cells/spots with higher expression (spiked cells) were located in one of those five  
92 patterns, hotspot, streak, circularity, bi-quarter circularity, and Purkinje layer in mouse cerebellum (Fig.  
93 1B). The distinctness of the pattern was determined by effect sizes, which were controlled by the fold  
94 change (FC) of expression in spiked cells compared to the background. The pattern size was determined by  
95 the percentage of spiked cells. Higher effect sizes and larger pattern sizes generated more distinct and bigger  
96 patterns, which were easier to be identified. Among the simulated genes, 500 genes display spatial patterns  
97 (details in the Methods section). The area under the curve (AUC) was used to measure the ability to  
98 distinguish between spatially and non-spatially variable genes.

99 We compared SpaGene with SpatialDE and SPARK-X. SpatialDE and SPARK-X both achieved high  
100 computational efficiency and good performance in other studies and SPARK-X is the only method  
101 applicable to data with sample size exceeding 30,000 (Zhu et al. 2021). As expected, effect sizes are the  
102 major factor affecting performance. Larger effect sizes produced more distinct patterns, which were easier  
103 to be distinguished from random spatial distributions and resulted in higher AUC values. For hotspot and  
104 streak patterns, SpaGene, SpatialDE, and SPARK-X successfully distinguished spatially from non-spatially  
105 variable genes when patterns were distinct (AUC=1 at  $FC \geq 5$  for hotspot and AUC=1 at  $FC \geq 8$  for streak  
106 patterns). For less distinct patterns, SpaGene performed slightly better than SpatialDE and SPARK-X for  
107 smaller patterns, which obtained AUC of 0.64, 0.52 and 0.55 for SpaGene, SPARK-X and SpatialDE  
108 respectively at  $FC=2$  and  $size=1$  in hotspot patterns, while SPARK-X outperformed SpatialDE and  
109 SpaGene for bigger patterns ( $size > 1$ ) (Fig. 1C). For circularity and bi-quarter circularity patterns, SpaGene  
110 achieved much better performance than SpatialDE and SPARK-X. For the circularity pattern, SpaGene  
111 achieved AUC of 0.99 even for the smallest pattern at  $FC=3$  and AUC of 1 at  $FC \geq 5$ . In comparison,  
112 SpatialDE only obtained AUC of 0.73 at  $FC=3$ , and SPARK-X failed to distinguish spatially from non-

113 spatially variable genes even at  $FC=5$  ( $AUC=0.5$ ) for the smallest pattern (size=1). SpaGene and SpatialDE  
114 achieved AUC of 1 while SPARK-X only obtained AUC of 0.72 at  $FC=8$  and size=1. Although the  
115 performance of SpatialDE and SPARK-X improved with increasing pattern sizes, SpaGene was more  
116 powerful than SpatialDE and SPARK-X (Fig. 1C). For the bi-quarter circularity pattern, SPARK-X failed  
117 even at the largest effect size for the two small patterns ( $AUC=0.5$  at  $FC=10$ , size=1 or 2), while SpaGene  
118 achieved  $AUC>=0.9$  and SpatialDE obtained AUC of 0.7-0.83 at  $FC>=3$  for any pattern sizes (Fig. 1C).  
119 For the Purkinje layer pattern, SPARK-X failed at any effect sizes ( $AUC=0.5$ ), while SpaGene achieved  
120 AUC of 0.81 at  $FC=2$ , 0.99 at  $FC=3$  and 1 at  $FC>=5$  (Fig. 1C). SpatialDE was not applied in this setting  
121 due to long computational time. To summarize, SpaGene achieved good performance for all spatial patterns,  
122 which obtained  $AUC>=0.98$  at  $FC>=3$  for relatively big patterns (size>1) and AUC close to 1 at  $FC>=5$  for  
123 any pattern sizes. In comparison, SPARK-X seemed to be very sensitive to pattern shapes, which worked  
124 well for hotspot and streak patterns, but not for circularity, bi-quarter circularity and Purkinje layer patterns  
125 even when patterns were strongly distinct from the background. Furthermore, SpaGene was more robust  
126 against pattern sizes than SpatialDE and especially SPARK-X, which sometimes showed more power to  
127 identify indistinct and large patterns than small distinct patterns. For example, SPARK-X obtained AUC  
128 of 0.8 at  $FC=3$  and size=3, but AUC of 0.7 even at  $FC=8$  and size=1 for circularity patterns. SpatialDE  
129 obtained AUC of 0.7 at  $FC=3$  and size=1, but 0.82 at  $FC=2$  and size=5 for bi-quarter circularity patterns.  
130 We also simulated scenarios with varying number of genes and cells/locations (Fig. S1-S5). We found that  
131 the performance of SpaGene were less dependent on the number of cells/locations compared to SpatialDE  
132 and SPARK-X. The evaluation on the simulation datasets sampled from real data obtained similar results  
133 (Fig. S6-S9).  
134 In terms of time complexity, SpaGene and SPARK-X are much more computationally efficient than  
135 SpatialDE. SpatialDE requires several orders of computational time than SpaGene and SPARK-X, and its  
136 runtime increases linearly or cubically with the number of genes and the number of cells/locations (Fig.  
137 S10A). For example, it takes SpatialDE 4,045 seconds to analyze a data with 10,000 genes and 5,000  
138 cells/location, while it only takes SpaGene and SPARKX 11 and 22 seconds, respectively (Fig. S10B).

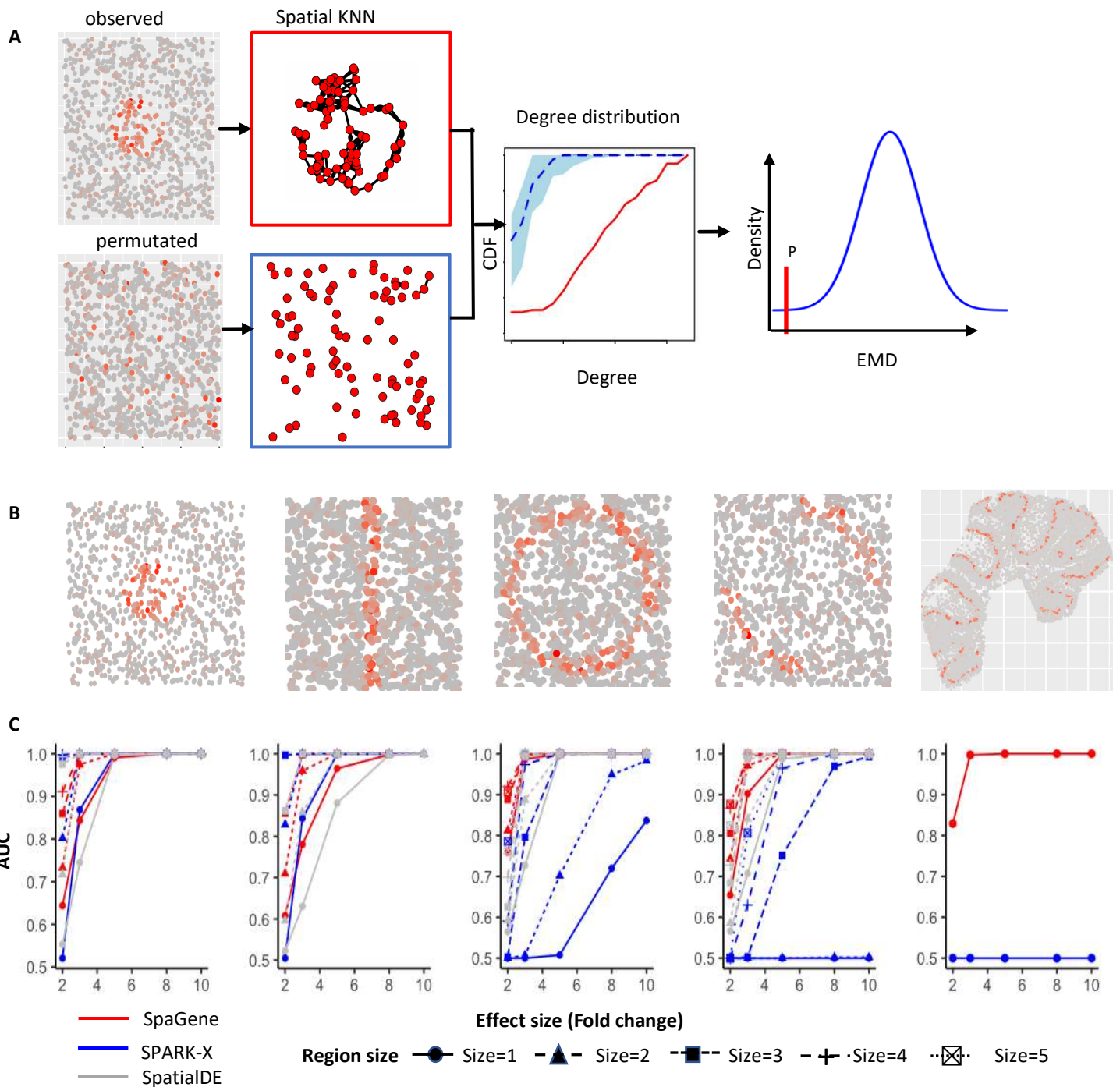


**Fig. 1. Schematic of SpaGene and simulation results.** A) Schematic of SpaGene; B) Visualization of five spatial patterns; C) AUC plots of SpaGene (red), SpatialDE (gray) and SPARK-X (blue) in simulated datasets with different effect sizes (x axis) and pattern sizes (point shapes) and 10,000 genes and 1,000 cells/locations. Simulated data were generated from negative binomial distributions.

140 **Application to MOB by spatial transcriptomics**

141 We applied SpaGene to spatial transcriptomics data from main olfactory bulb (MOB) (Stahl et al. 2016),  
142 involving 16,218 genes measured on 262 spots. The MOB has a roughly concentric arrangement of seven  
143 cell layers (Nagayama et al. 2014). SpaGene identified 634 as spatially variable genes (adjusted p-value,  
144  $\text{adjp}<0.05$ ), including genes known to be located in specific layers. Several examples were shown in Fig.  
145 2A, such as *Pcp4* in Granule cell layer (GCL) ( $\text{adjp}=3\text{e-}6$ ) (Sangameswaran et al. 1989), *Slc17a7* in Mitral  
146 cell layer (MCL) ( $\text{adjp}=7\text{e-}4$ ) (Zhang et al. 2021), *Cck* in Glomerular layer (GL) ( $\text{adjp}=2\text{e-}3$ ) (Sun et al.  
147 2020b), *Serpine2* in External plexiform layer (EPL) ( $\text{adjp}=4\text{e-}3$ ) (Mansuy et al. 1993) and *Fabp7* in  
148 Olfactory nerve layer (ONL) ( $\text{adjp}=4\text{e-}76$ ) (Young et al. 2013). Based on those identified spatially variable  
149 genes, SpaGene successfully reconstructed the underlying seven-layered MOB structure (Fig. S11). To be  
150 noted, SpaGene identified a pattern corresponding to subependymal zone (SEZ) (pattern 4 in Fig. S11).  
151 SEZ was unidentifiable by spatially unaware single-cell clustering, which only discovered five distinct  
152 clusters (Fig. S12A). SEZ harbors neural stem cells. *Sp9* is the top gene specifically located in SEZ, which  
153 is a transcription factor that regulate MOB interneuron development (Li et al. 2018).

154 We compared SpaGene with SPARK-X and SpatialDE. Overall, SpaGene and SpatialDE had more  
155 overlapping than SPARK-X (Fig. S12B). We ranked spatially variable genes by each method and carefully  
156 examined those genes identified to be very significant by one method but insignificant by another method.  
157 First, we ranked genes by SpaGene and listed the top 6 genes with inconsistent results (Fig. S13). *Kif5b*,  
158 *Atf5*, *Sorbs1*, *Piekhb1* and *Mfap3l* were detected to be very significant by SpaGene ( $\text{adjp}<\text{e-}21$ ), which were  
159 all specifically expressed in ONL (Fig. S11). However, none of them were found by SPARK-X, while *Atf5*,  
160 *Piekhb1* and *Mfap3l* were undiscovered by SpatialDE (Fig. S13). Another gene, *Grb2* was identified by  
161 SPARK-X but missed by SpatialDE, showing a very clear GCL pattern (Fig. S13). Then we ranked genes  
162 by SPARK-X and checked the top 6 inconsistent ones (Fig. S14). *Camk2a*, *Psd3*, *Meis2*, *Calm2*, *Arf3* and  
163 *Stxbp1* ranked high by SPARK-X, which displayed strong GCL patterns. All were identified by SpaGene  
164 but none by SpatialDE, indicating SpatialDE had limited power in identifying GCL-specific genes (Fig.  
165 S14). Finally, we ranked genes by SpatialDE and examined the top 6 inconsistent ones, including *Spem1*,

166 *Siglec1*, *Cck*, *Kif5b*, *Apoe*, and *Il12a* (Fig. S15). *Spem1*, *Siglec1*, and *Il12a*, however, only expressed in one  
 167 or two spots, which were likely to be false signals. *Cck*, *Kif5b* and *Apoe* exhibited GL or ONL patterns,  
 168 which were identified by SpaGene but missed by SPARK-X (Fig. S15). These comparisons demonstrated  
 169 that SpaGene successfully identified genes with visually distinct patterns, while SPARK-X and SpatialDE  
 170 missed several genes in certain layers even they showed distinct patterns.

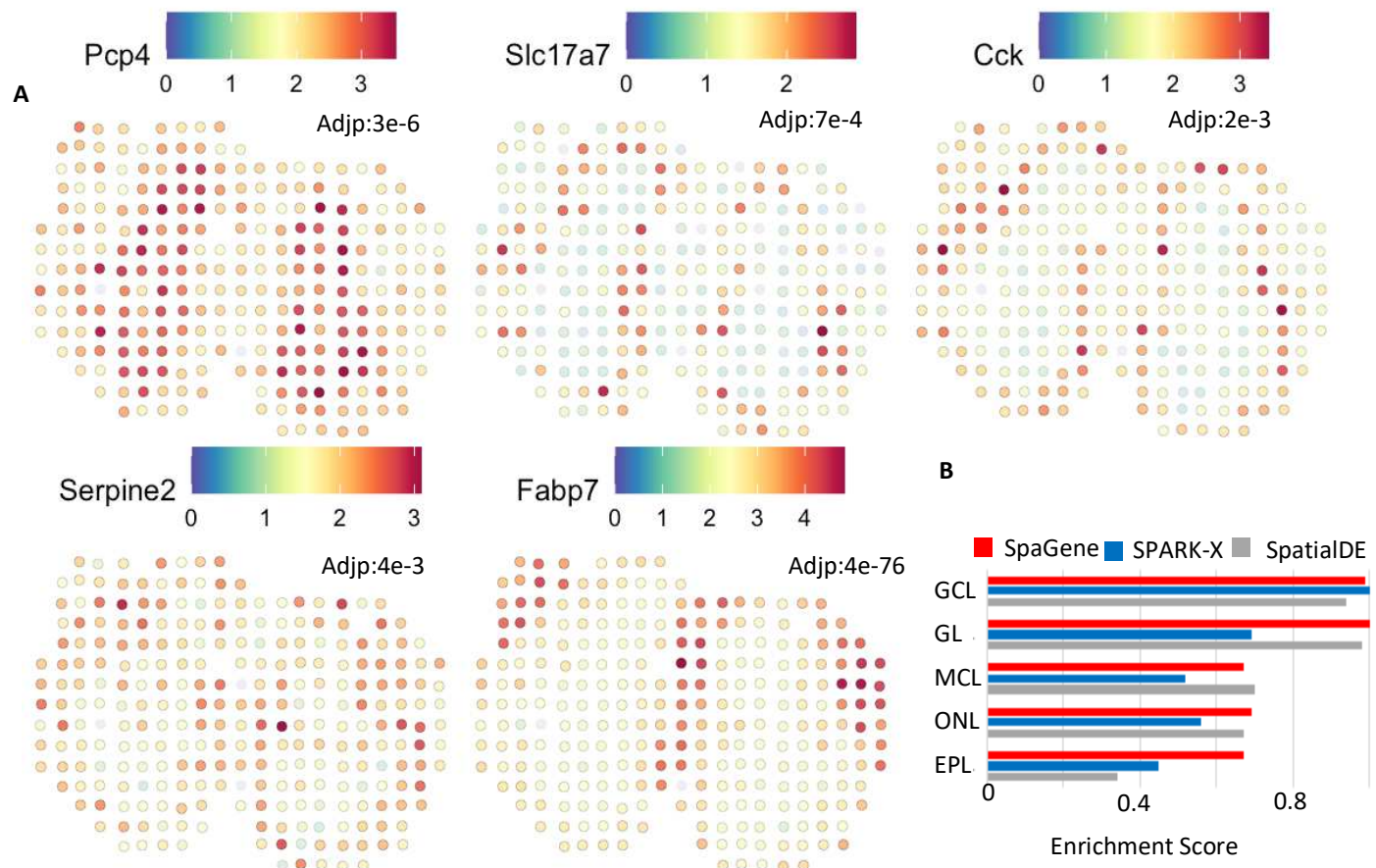


**Fig. 2. Application of SpaGene to spatial transcriptomics of main olfactory bulb data (MOB).** A) Visualization of five known spatially variable genes located in specific MOB layers (high expression in red, and low in blue), with adjusted p-values from SpaGene; B) Enrichment scores of markers in location-restricted cell types by SpaGene, SpatialDE and SPARK-X.

171 Since spatially unaware single-cell clustering uncovered cell types located in MOB layers, we expected that  
 172 top markers in each layer-specific cell type would be identified as spatially variable genes. We calculated  
 173 scores to measure the enrichment of those top markers in SpaGene, SPARK-X and SpatialDE. SpaGene  
 174 obtained high enrichment scores in all layers, suggesting it successfully identified all layer-specific marker

175 genes as being very significant. In contrast, SPARK-X obtained high in GCL layers but low in other layers.  
176 SpatialDE achieved high scores in Mitral cell layer , but relatively low scores in GCL and EPL layers (Fig.  
177 2C).

178

### 179 **Application to mouse preoptic hypothalamus by MERFISH**

180 We applied SpaGene to mouse preoptic hypothalamus data by MERFISH (Moffitt et al. 2018), consisting  
181 of 161 genes measured on 5,665 cells . The 161 genes include 156 pre-selected markers of distinct cell  
182 populations and five blank control genes. Spatially unaware single-cell clustering identified multiple cell  
183 types, most of which were spatially localized in specific regions, such as mature oligodendrocyte (OD),  
184 ependymal, mural and some inhibitory and excitatory neuron cell types (Fig. 3A). SpaGene identified those  
185 markers from region-specific cell types as top variable genes. Some representative genes were shown in  
186 Fig. 3B, such as *Ntng1* in inhibitory neurons (adjp=5e-108), *Mbp* in mature OD (adjp=0), *Cd24a* in  
187 Ependymal (adjp=0), *Adcyap1* in excitatory neurons (adjp=0), and *Myh11* in Mural cells (adjp=4e-24).  
188 Comparing SpaGene with SPARK-X and SpatialDE, we found their results were highly correlated in terms  
189 of significance (R=0.91 between SpaGene and SpatialDE, R=0.7 between SpaGene and SPARK-X, and  
190 R=0.8 between SPARK-X and SpatialDE) (Fig. 3C). We also compared the number of positive genes given  
191 the number of negative control genes identified (Fig. 3D). The results supported a higher power of SpaGene.  
192 For example, SpaGene detected 149 true positives, while SpatialDE discovered 144 and SPARKX revealed  
193 128, when one negative control was detected (one false positive).

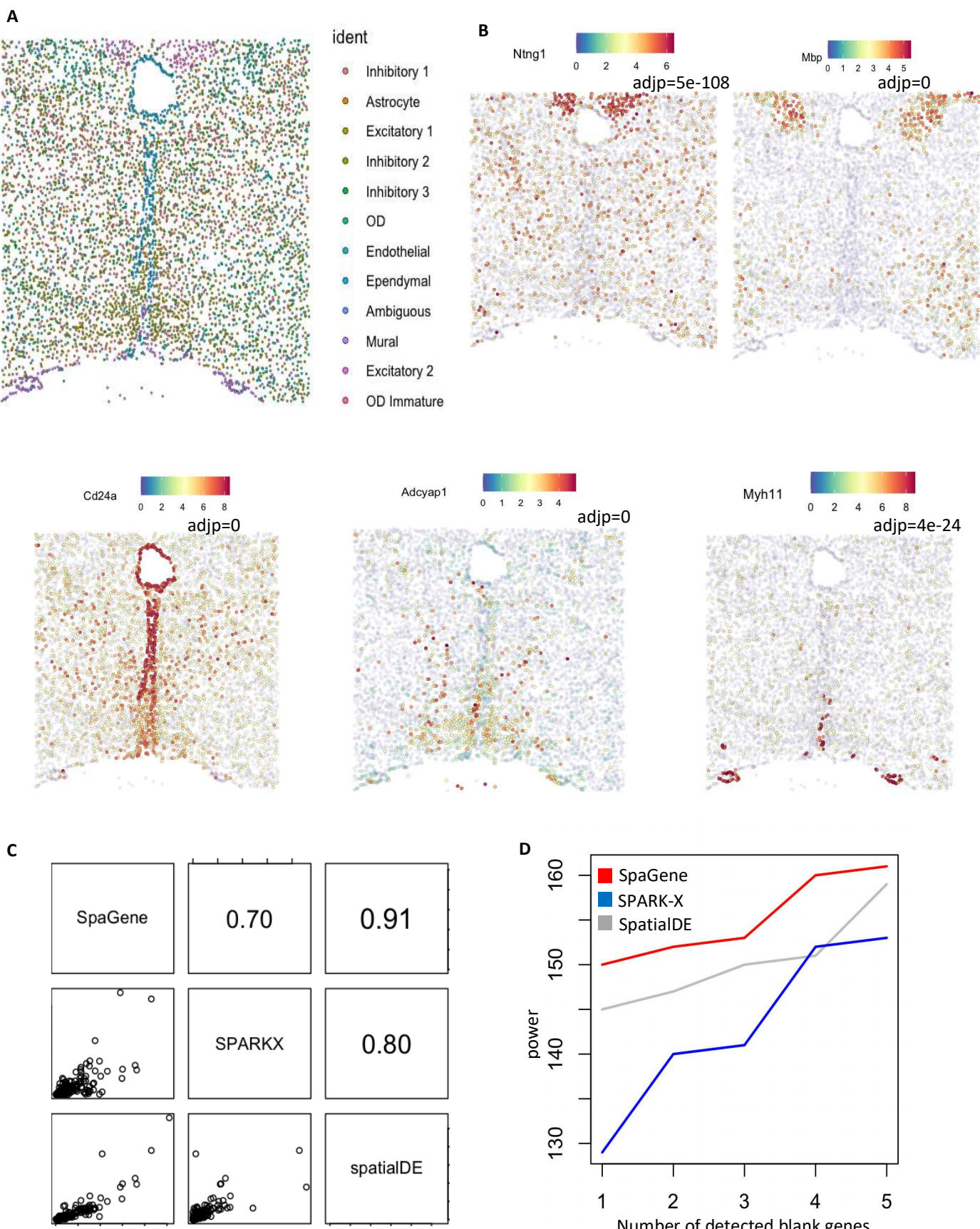


**Fig. 3. Application of SpaGene to MERFISH of mouse preoptic hypothalamus data.** A) Spatially-unaware cell clustering; B) Visualization of five spatial variable genes (high expression in red and low in blue) with adjusted p-values from SpaGene; C) Pairwise correlation of results from SpaGene, SpatialDE and SPARK-X; D) Power plot shows the number of genes with spatial expression pattern (y axis) identified by SpaGene, SpatialDE and SPARK-X versus the number of blank control genes identified at the same threshold.

195 **Application to mouse cerebellum by Slideseq V2**

196 We applied SpaGene to mouse cerebellum data by Slideseq V2 (Stickels et al. 2021), containing 20,141  
197 genes measured on 11,626 spots. SpaGene identified 619 genes with spatial patterns ( $adjp < 0.05$ ). The  
198 cerebellum is made of three layers, molecular, Purkinje and granular layers from outer to inner, and white  
199 matter underneath. SpaGene detected genes, known to be specifically located in three layers and white  
200 matter, to be very significant, such as *Kcnd2* in granular layer ( $adjp = 4e-253$ ) (Varga et al. 2000), *Car8* in  
201 Purkinje layer ( $adjp = 0$ ) (Miterko et al. 2019), *Gad1* in molecular layer ( $adjp = 2e-64$ ) (Kirsch et al. 2012)  
202 and *Mbp* in white matter ( $adjp = 0$ ) (Verity and Campagnoni 1988) (Fig. 4A). Based on those identified  
203 spatially variable genes, SpaGene successfully reconstructed the tightly folded layer structure of cerebellum.  
204 Patterns 1 and 3 corresponded to granular layer, patterns 2, 6 and 8 represented molecular layer, patterns 4  
205 and 5 stood for Bergmann glia and purkinje neurons in Purkinje layer, and pattern 7 imaged white matter  
206 (Fig. S16).

207 We compared SpaGene with SPARK-X but not SpatialDE because it would take hours to analyze such  
208 large-scale data. SPARK-X discovered 530 genes, while 230 overlapped with SpaGene (Fig. S17). We  
209 examined carefully at those genes detected to be very significant by one method but insignificant by the  
210 other one (Fig. S17). Those genes specifically located in Purkinje layer, such as *Car8*, *Itpr1*, *Pcp2*, and  
211 *Pcp4*, were detected as being the most significant by SpaGene ( $adjp = 0$ ) but undetected by SPARK-X,  
212 suggesting SPARK-X had limited power to identify the Purkinje pattern (Fig. S18). In comparison,  
213 *Catsperd*, *Ifit3*, and *Ptprt* ranked top by SPARK-X, but undetected by SpaGene, which didn't seem to have  
214 obvious patterns (Fig. S19). SpaGene obtained the significance of *Mog* were just below the cutoff  
215 ( $adjp = 0.05$ ), which seemed to be dispersed in the white matter (Fig. S19).

216 Spatially unaware single-cell clustering found localized cell types, such as molecular layer neurons,  
217 purkinje neurons in the purkinje layer, granule cells in the granule layer (Fig. 4B) . We expected markers  
218 in those spatially-restricted cell types were identified and ranked top by the methods. The enrichment  
219 analysis found that SpaGene obtained high enrichment scores in all three layers, while SPARK-X got a

220 high score in granular layer, but low scores in other two layers, especially in the Purkinje layer. This result  
221 further demonstrated that SpaGene is more robust to any spatial patterns (Fig. 4C).  
222

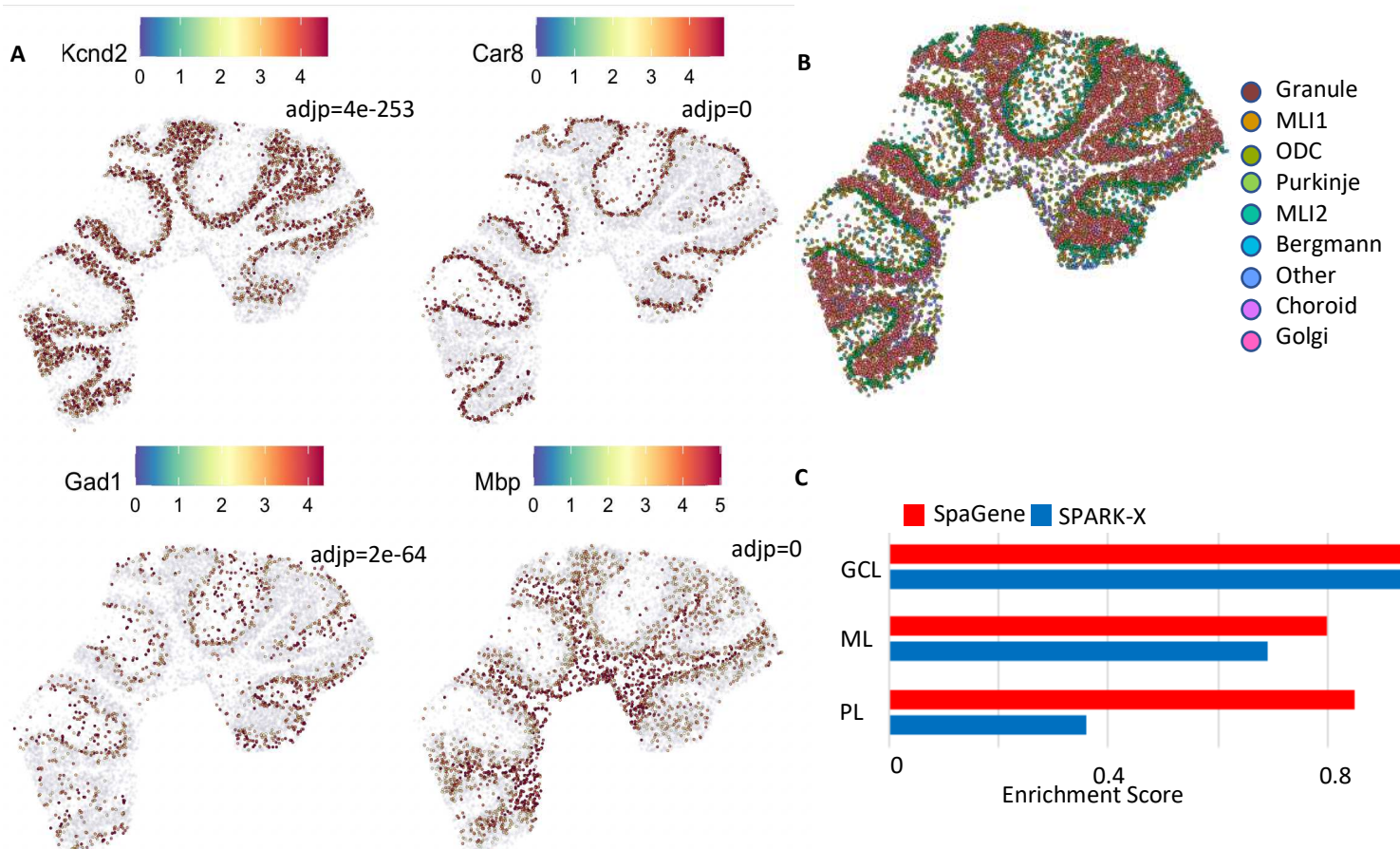


**Fig. 4. Application of SpaGene to Slideseq V2 of mouse cerebellum data.** A) Visualization of four known spatially variable genes located in specific cerebellum layers (high expression in red, and low in blue), with adjusted p-values from SpaGene; B) Spatially unaware cell clustering; C) Enrichment scores of markers in location-restricted cell types by SpaGene and SPARK-X.

### 223 Application to MOB by HDST

224 We applied SpaGene to olfactory bulb from high-definition spatial transcriptomics (HDST) (Vickovic et al.  
225 2019), involving 19,950 genes measured on 181,367 spots. HDST is extremely sparse, where only 21 spots  
226 have more than 50 genes detected. In this case, SpaGene used an adaptive strategy to expand the  
227 neighborhood search for genes with high sparsity. SpaGene identified 249 genes as being spatially variable.

228 The most significant genes included *Ptgds* (adjp=1e-232), *Gphn* (adjp=3e-114) and *Camk1d* (adjp=3e-61).  
229 Although spatial patterns of those genes were not visually distinct due to high sparsity of the HDST data,  
230 there were vague patterns showing *Ptgds* localized in ONL, *Gphn* in MCL and EPL, and *Camk1d* in GCL  
231 (Fig. 5A). Those specific localizations have been reported before (Rees et al. 2003; Perera et al. 2020) and  
232 validated by in situ hybridization in the Allen Brain Atlas (Fig. 5B).  
233 We compared SpaGene with SPARK-X but not SpatialDE because it would take months to analyze such  
234 large-scale data. SPARK-X detected 133 genes, which overlapped significantly with SpaGene (90 in  
235 common). Among the 40 genes most associated with each MOB layer (top 5 genes in eight patterns in Fig.  
236 S11), SpaGene found 12 genes (*Ptgds*, *Fabp7*, *Gad1*, *Vtn*, *Kctd12*, *Kif5b*, *Apod*, *Pcp4*, *Gpsm1*, *Slc1a2*,  
237 *Nrgn*, and *Map1b*), while SPARK-X only detected six (*Ptgds*, *Fabp7*, *Kctd12*, *Kif5b*, *Apod*, and *Pcp4*).  
238  
239  
240

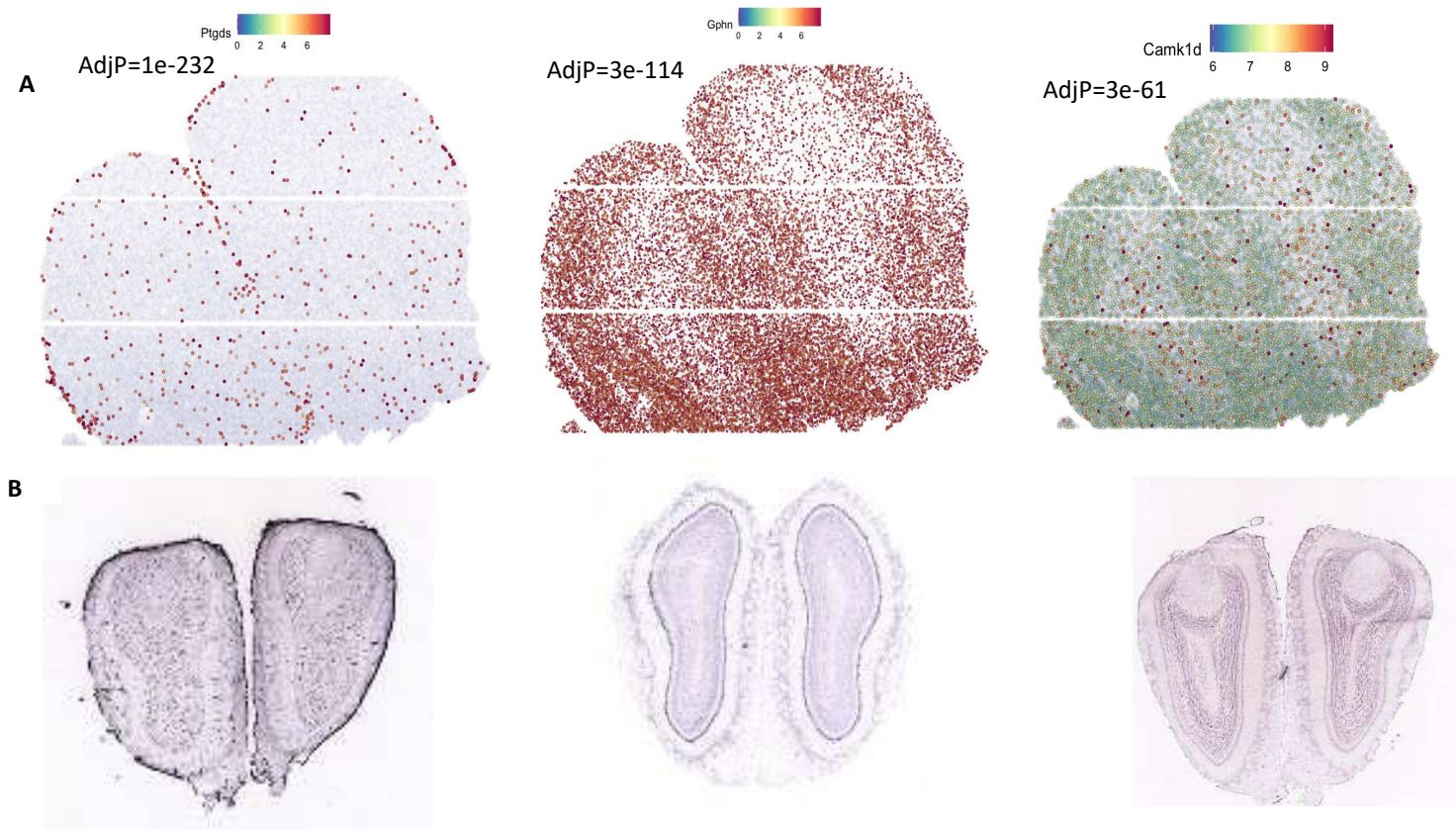


**Fig. 5. Application of SpaGene to HDST of MOB data.** Visualization of three spatially variable genes. A) gene-expression levels from HDST (high in red, low in blue), with adjusted p-values from SpaGene; B) *in situ* hybridization results for the three genes obtained from the Allen Brain Atlas.

241 **Identification of spatially colocalized ligand-receptor pairs**

242 We extended SpaGene to identify cell-cell communications mediated by colocalized ligand and receptor  
 243 pairs. SpaGene found 35 ligand-receptor interactions from the mob data by spatial transcriptomics. The two  
 244 most significant ligand-receptor pairs were *Igfbp5-Cav1* (adjp=3e-31) and *Apoe-Lrp6* (adjp=1e-18), both  
 245 happening between ONL and GL. *Apoe* is known to be enriched in ONL and GL and also identified to be  
 246 very significant by SpaGene (adjp=1e-50). Most spots with high *Apoe* expression were surrounded with  
 247 spots with high *Lrp6* expression (Fig.6A), suggesting potential interactions between them. *Apoe-Lrp6*  
 248 mediates Wnt signaling, which is important for the regulation of synaptic integrity and cognition (Zhao et  
 249 al. 2018). The identification of *Apoe-Lrp6* between ONL and GL layers might be suggestive of the potential  
 250 regulation of Wnt signaling in the establishment of periphery–CNS olfactory connections.

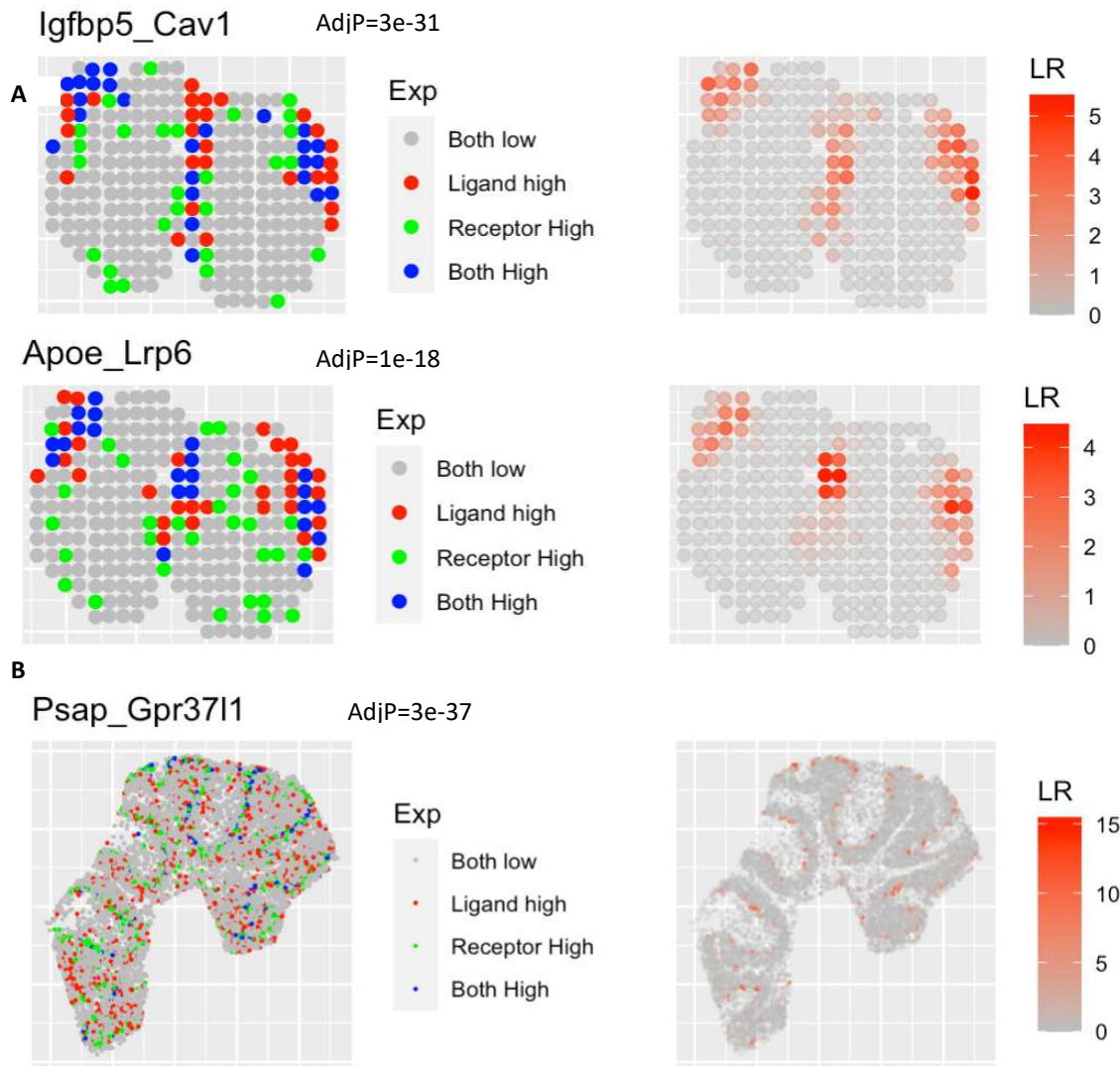


**Fig. 6. Extension of SpaGene to identify ligand-receptor interactions.** A) Visualization of Igfbp5-Cav1 and Apoe-Lrp6 interactions for ST MOB data, with adjusted p-values from SpaGene. B) Visualization of the Psap-Gpr37l1 interaction for Slideseq V2 mouse cerebellum data, with the adjusted p-value from SpaGene. Left is the relative expression of the ligand and the receptor, right is the interaction strength.

252 SpaGene found 13 ligand-receptor interactions from the mouse cerebellum data by Slideseq V2. The most  
 253 significant pair was Psap-Gpr37l1 ( $adjp=1e-27$ ) (Fig. 6B). Gpr37l1 was known to be strongly expressed in  
 254 Purkinje layer and also identified by SpaGene ( $adjp=8e-130$ ). *Psap*, in contrast, was not as specifically  
 255 localized as *Gpr37l1* ( $adjp=6e-8$ ). Psap-Gpr37l1 protects neural cells from cellular damage (Li et al. 2017).  
 256 The identification of Psap-Gpr37l1 between Purkinje layer and surrounding layers further supports its

257 important role in brain function. Additionally, Ptn-Pptrz1, identified as the only interaction by MERRINGUE  
258 (Miller et al. 2021), ranked the top four by SpaGene (adjp=2e-7).

259

## 260 **DISCUSSION**

261 Recent advances in spatial omics technologies increase the demand for scalable and robust methods to  
262 characterize spatially variable patterns. Here, we developed SpaGene, a fast and model-free method to  
263 identify spatially variable genes. SpaGene has been extensively evaluated on seven datasets generated from  
264 a variety of spatial technologies, ranging from low to high throughput and spatial resolution. Additional  
265 analyses on breast cancer from spatial transcriptomics, mouse brain from 10X Visium, and olfactory bulb  
266 from Slide-seqV2 were shown in Supplementary Figures S20-S30. The results consistently demonstrated  
267 that SpaGene successfully identified known spatially variable genes and also markers in spatially-restricted  
268 cell clusters. Simple factor analysis on those identified genes reconstructed underlying tissue structures,  
269 further demonstrating the ability of SpaGene to characterizing spatial patterns.

270 Compared with existing approaches, SpaGene is more robust to pattern shapes, data distribution and  
271 sparsity, non-uniform cellular densities, and the number of spatial locations. The power of SpatialDE,  
272 SPARK and SPARK-X highly depend on spatial covariance models, that is, how well those predefined  
273 kernel functions match the true underlying spatial patterns. Moreover, SpatialDE and SPARK use  
274 parametric modeling based on the assumption of spatial data following Gaussian or Poisson distributions.  
275 Therefore, their performance would be compromised significantly for those genes whose expression  
276 misalign the model defined by those kernel functions and whose distribution violate Gaussian or Poisson  
277 distributions. SpaGene, in contrast, is a model-free and distribution-free method. Without any assumption,  
278 SpaGene is able to identify any spatial patterns and applied on any spatial omics data, such as identification  
279 of spatially localized clones and histone markers in spatial genomics and epigenomics data. The  
280 significance from SpaGene reflects the distinctness of spatial patterns rather than the extent of match to the  
281 defined model. SpaGene uses neighborhood graphs to represent spatial connections, making it more robust  
282 to non-uniform cellular densities common in tissues. Furthermore, SpaGene is highly computationally

283 efficient. It only took seconds to minutes for SpaGene to analyze large-scale spatial transcriptomics data,  
284 which required hours, days or even months for most methods (Zhu et al. 2021) (Fig. S10C).  
285 SpaGene is very flexible, which can tune neighborhood search spaces automatically based on the data  
286 sparsity. SpaGene can incorporate the cell type information to find spatially variable genes within the same  
287 cell type. For example, SpaGene identified *Aldoc* as the most spatially variable genes within the Purkinje  
288 layer (adjp=4e-90) (the function SpaGene\_CT was provided in the package), which has been demonstrated  
289 to show a regional enrichment pattern that was consistent with the known paths of parasagittal stripes across  
290 individual lobules (Kozareva et al. 2021). Furthermore, SpaGene was easily extended to find colocalized  
291 gene pairs. It successfully identified Psap-Gpr3711 and Ptn-Ptprz1 in mouse cerebellum, and Fn1-Cd44 in  
292 invasive breast cancer regions (Fig. S30). The default neighborhood search regions could be further  
293 adjusted to identify those long-distance interactions. In summary, SpaGene is very powerful tool to  
294 characterize any localized and co-localized patterns. Potential extensions of SpaGene to find alterations in  
295 spatial patterns across conditions would further expands its application.

296

## 297 METHODS

### 298 Method overview

299 Spatially variable genes are those with uneven spatial distribution of expression, where cells/spots with  
300 high expression are more likely to be spatially connected than random. Given a set of spatial locations,  
301 SpaGene first builds the spatial network using k-nearest neighbors. SpaGene then quantifies the spatial  
302 connection of cells/spots with high expression by their degree distribution. Finally SpaGene compares the  
303 observed spatial connection with those from random permutations (Fig. 1A). Genes with significantly  
304 higher spatial connection than random are identified as spatially variable genes.

305 The degree distribution  $p(i)$  is defined to be the fraction of cells/spots with degree of  $i$ . Earth mover's  
306 distance (*EMD*) is used to quantify the distance from the observed degree distribution to a distribution from  
307 a fully connected network. Smaller EMD distances indicate higher spatial connection.

308

$$EMD = \sum_{i=0}^{2*k} p(i)(2*k - i)$$

309 To generate the null distribution of *EMD*, the same number of cells/spots is randomly sampled and the  
310 spatial connection of those cells/spots is quantified as *EMD'*. The mean and the standard deviation of  
311 *EMD'* is estimated after 5,00 random permutations. The observed *EMD* is compared to the null distribution  
312 of *EMD'* to evaluate its significance.

313

$$p(x > EMD) = p(z < \frac{EMD - \text{mean}(EMD')}{Sd(EMD')})$$

314

315 **Identification of spatial patterns**

316 Non-negative matrix factorization is applied on spatially variable genes detected by SpaGene to identify  
317 distinct spatial patterns. NMF is implemented by the RcppML R package. The Spearman correlation  
318 between expression of spatially variable genes and cells/spots factor matrix from NMF is used to find the  
319 most representative genes in each pattern.

320

321 **Simulation designs**

322 We followed simulation designs of SPARK-X and Trendsceek. Briefly we generated two datasets with five  
323 spatial expression patterns, local hotspot, streak, circularity, bi-quarter circularity and mouse purkinje layer.  
324 For the first four patterns, spatial locations of cells were generated by a random-point-pattern Poisson  
325 process. The spatial locations of the pattern of mouse purkinje layer was obtained from Slideseq V2 mouse  
326 cerebellum data. The expression values were either generated from negative binomial distributions  
327 following SPARK-X or bootstrap-sampled from spatial transcriptomics MOB data following Trendsceek.  
328 Simulation datasets varied on a number of parameters: 1) the number of genes varied from 1000, 3000, and  
329 10,000, among of which 500 genes are spatially variable; 2) the number of cells varied from 300, 1000,  
330 2000 and 5000 except for the purkinje layer pattern; 3) the fold change of expression in the spatial region  
331 compared to those in the background; For the negative binomial distribution, the fold change varied from

332 2, 3,5, 8 to 10. For the resampled real dataset, the expression of spiked cells were generated from 65%,  
333 70%, 80% to 90% quantile of the expression distribution; 4) the number of spiked cells except for the  
334 purkinje layer pattern. For the hotspot and the streak patterns, the percentage of spiked cells varied from  
335 5%, 10%, 20% to 30%. For the circularity and bi-quarter circularity patterns, the width of circularity varied  
336 between 0.05, 0.075, 0.1, 0.125 and 0.15.

337

### 338 **Spatial transcriptomics datasets**

339 SpaGene was applied on seven spatial transcriptomics datasets, covering a variety of platforms with low  
340 and high throughput and spatial resolution. Two spatial transcriptomics data from mouse olfactory bulb  
341 and human breast cancer contained genome-wide expression profiles on only hundreds of spots (low spatial  
342 resolution) (Stahl et al. 2016). MERFISH on the mouse preoptic region of the hypothalamus targeted only  
343 160 genes at single cell resolution. 10X Visium on the mouse brain comprised of whole transcriptomics on  
344 thousands of spots with a spatial resolution of 55  $\mu$ m. Two Slideseq V2 from mouse cerebellum and  
345 olfactory bulb contained whole transcriptomics on tens of thousands of spots with a spatial resolution of 10  
346  $\mu$ m. HDST from mouse olfactory bulb measured whole transcriptomics on hundreds of thousands of spots  
347 with a spatial resolution of 2 $\mu$ m.

348

### 349 **DATA ACCESS**

350 Seven spatial transcriptomics data were available from original studies and also from the SpaGene Github  
351 repository <https://github.com/liuqivandy/SpaGene> . In addition to identification of spatially variable genes  
352 and patterns, the R package SpaGene also provides functions to visualize spatial patterns and co-localized  
353 ligand-receptor pairs. Vignettes on seven spatial transcriptomics data with raw data, codes and results,  
354 including spatial variable genes identification, pattern identification and visualization, co-localized ligand-  
355 receptor pairs identification and visualization, are also available at the GitHub.

356

### 357 **COMPETING INTEREST STATEMENT**

358 The authors declare no competing interests.  
359

360 **ACKNOWLEDGMENTS**

361 This work is supported by National Cancer Institute grants (U2C CA233291 and U54 CA217450), and  
362 Cancer Center Support Grant (P30CA068485).

363  
364 **REFERENCES**

366 Anderson A, Lundeberg J. 2021. sepal: Identifying Transcript Profiles with Spatial Patterns by  
367 Diffusion-based Modeling. *Bioinformatics* doi:10.1093/bioinformatics/btab164.

368 Atta L, Fan J. 2021. Computational challenges and opportunities in spatially resolved  
369 transcriptomic data analysis. *Nat Commun* **12**: 5283.

370 Deng Y, Bartosovic M, Kukanja P, Zhang D, Liu Y, Su G, Enninful A, Bai Z, Castelo-Branco G, Fan  
371 R. 2022. Spatial-CUT&Tag: Spatially resolved chromatin modification profiling at the  
372 cellular level. *Science* **375**: 681-686.

373 Dhainaut M, Rose SA, Akturk G, Wroblewska A, Nielsen SR, Park ES, Buckup M, Roudko V, Pia L,  
374 Sweeney R et al. 2022. Spatial CRISPR genomics identifies regulators of the tumor  
375 microenvironment. *Cell* doi:10.1016/j.cell.2022.02.015.

376 Edsgard D, Johnsson P, Sandberg R. 2018. Identification of spatial expression trends in single-  
377 cell gene expression data. *Nat Methods* **15**: 339-342.

378 Kirsch L, Liscovitch N, Chechik G. 2012. Localizing genes to cerebellar layers by classifying ISH  
379 images. *PLoS Comput Biol* **8**: e1002790.

380 Kozareva V, Martin C, Osorno T, Rudolph S, Guo C, Vanderburg C, Nadaf N, Regev A, Regehr  
381 WG, Macosko E. 2021. A transcriptomic atlas of mouse cerebellar cortex  
382 comprehensively defines cell types. *Nature* **598**: 214-219.

383 Larsson L, Frisen J, Lundeberg J. 2021. Spatially resolved transcriptomics adds a new dimension  
384 to genomics. *Nat Methods* **18**: 15-18.

385 Lewis SM, Asselin-Labat ML, Nguyen Q, Berthelet J, Tan X, Wimmer VC, Merino D, Rogers KL,  
386 Naik SH. 2021. Spatial omics and multiplexed imaging to explore cancer biology. *Nat  
387 Methods* **18**: 997-1012.

388 Li J, Wang C, Zhang Z, Wen Y, An L, Liang Q, Xu Z, Wei S, Li W, Guo T et al. 2018. Transcription  
389 Factors Sp8 and Sp9 Coordinateley Regulate Olfactory Bulb Interneuron Development.  
390 *Cereb Cortex* **28**: 3278-3294.

391 Li X, Nabeka H, Saito S, Shimokawa T, Khan MSI, Yamamiya K, Shan F, Gao H, Li C, Matsuda S.  
392 2017. Expression of prosaposin and its receptors in the rat cerebellum after kainic acid  
393 injection. *IBRO Rep* **2**: 31-40.

394 Longo SK, Guo MG, Ji AL, Khavari PA. 2021. Integrating single-cell and spatial transcriptomics to  
395 elucidate intercellular tissue dynamics. *Nat Rev Genet* **22**: 627-644.

396 Mansuy IM, van der Putten H, Schmid P, Meins M, Botteri FM, Monard D. 1993. Variable and  
397 multiple expression of Protease Nexin-1 during mouse organogenesis and nervous  
398 system development. *Development* **119**: 1119-1134.

399 Marx V. 2021. Method of the Year: spatially resolved transcriptomics. *Nat Methods* **18**: 9-14.

400 Miller BF, Bambah-Mukku D, Dulac C, Zhuang X, Fan J. 2021. Characterizing spatial gene  
401 expression heterogeneity in spatially resolved single-cell transcriptomic data with  
402 nonuniform cellular densities. *Genome Res* **31**: 1843-1855.

403 Miterko LN, White JJ, Lin T, Brown AM, O'Donovan KJ, Sillitoe RV. 2019. Persistent motor  
404 dysfunction despite homeostatic rescue of cerebellar morphogenesis in the Car8  
405 waddles mutant mouse. *Neural Dev* **14**: 6.

406 Moffitt JR, Bambah-Mukku D, Eichhorn SW, Vaughn E, Shekhar K, Perez JD, Rubinstein ND, Hao  
407 J, Regev A, Dulac C et al. 2018. Molecular, spatial, and functional single-cell profiling of  
408 the hypothalamic preoptic region. *Science* **362**.

409 Nagayama S, Homma R, Imamura F. 2014. Neuronal organization of olfactory bulb circuits.  
410 *Front Neural Circuits* **8**: 98.

411 Perera SN, Williams RM, Lyne R, Stubbs O, Buehler DP, Sauka-Spengler T, Noda M, Micklem G,  
412 Southard-Smith EM, Baker CVH. 2020. Insights into olfactory ensheathing cell  
413 development from a laser-microdissection and transcriptome-profiling approach. *Glia*  
414 **68**: 2550-2584.

415 Ratz M, von Berlin L, Larsson L, Martin M, Westholm JO, La Manno G, Lundeberg J, Frisen J.  
416 2022. Clonal relations in the mouse brain revealed by single-cell and spatial  
417 transcriptomics. *Nat Neurosci* **25**: 285-294.

418 Rees MI, Harvey K, Ward H, White JH, Evans L, Duguid IC, Hsu CC, Coleman SL, Miller J, Baer K et  
419 al. 2003. Isoform heterogeneity of the human gephyrin gene (GPHN), binding domains  
420 to the glycine receptor, and mutation analysis in hyperekplexia. *J Biol Chem* **278**: 24688-  
421 24696.

422 Sangameswaran L, Hempstead J, Morgan JI. 1989. Molecular cloning of a neuron-specific  
423 transcript and its regulation during normal and aberrant cerebellar development. *Proc  
424 Natl Acad Sci U S A* **86**: 5651-5655.

425 Stahl PL, Salmen F, Vickovic S, Lundmark A, Navarro JF, Magnusson J, Giacomello S, Asp M,  
426 Westholm JO, Huss M et al. 2016. Visualization and analysis of gene expression in tissue  
427 sections by spatial transcriptomics. *Science* **353**: 78-82.

428 Stickels RR, Murray E, Kumar P, Li J, Marshall JL, Di Bella DJ, Arlotta P, Macosko EZ, Chen F.  
429 2021. Highly sensitive spatial transcriptomics at near-cellular resolution with Slide-  
430 seqV2. *Nat Biotechnol* **39**: 313-319.

431 Sun S, Zhu J, Zhou X. 2020a. Statistical analysis of spatial expression patterns for spatially  
432 resolved transcriptomic studies. *Nat Methods* **17**: 193-200.

433 Sun X, Liu X, Starr ER, Liu S. 2020b. CCKergic Tufted Cells Differentially Drive Two Anatomically  
434 Segregated Inhibitory Circuits in the Mouse Olfactory Bulb. *J Neurosci* **40**: 6189-6206.

435 Svensson V, Teichmann SA, Stegle O. 2018. SpatialDE: identification of spatially variable genes.  
436 *Nat Methods* **15**: 343-346.

437 Varga AW, Anderson AE, Adams JP, Vogel H, Sweatt JD. 2000. Input-specific immunolocalization  
438 of differentially phosphorylated Kv4.2 in the mouse brain. *Learn Mem* **7**: 321-332.

439 Verity AN, Campagnoni AT. 1988. Regional expression of myelin protein genes in the developing  
440 mouse brain: *in situ* hybridization studies. *J Neurosci Res* **21**: 238-248.

441 Vickovic S, Eraslan G, Salmen F, Klughammer J, Stenbeck L, Schapiro D, Aijo T, Bonneau R,  
442 Bergenstrahle L, Navarro JF et al. 2019. High-definition spatial transcriptomics for in situ  
443 tissue profiling. *Nat Methods* **16**: 987-990.

444 Young JK, Heinbockel T, Gondre-Lewis MC. 2013. Astrocyte fatty acid binding protein-7 is a  
445 marker for neurogenic niches in the rat hippocampus. *Hippocampus* **23**: 1476-1483.

446 Zhang L, Hernandez VS, Gerfen CR, Jiang SZ, Zavala L, Barrio RA, Eiden LE. 2021. Behavioral role  
447 of PACAP signaling reflects its selective distribution in glutamatergic and GABAergic  
448 neuronal subpopulations. *Elife* **10**.

449 Zhao N, Liu CC, Qiao W, Bu G. 2018. Apolipoprotein E, Receptors, and Modulation of  
450 Alzheimer's Disease. *Biol Psychiatry* **83**: 347-357.

451 Zhao T, Chiang ZD, Morris JW, LaFave LM, Murray EM, Del Priore I, Meli K, Lareau CA, Nadaf  
452 NM, Li J et al. 2022. Spatial genomics enables multi-modal study of clonal heterogeneity  
453 in tissues. *Nature* **601**: 85-91.

454 Zhu J, Sun S, Zhou X. 2021. SPARK-X: non-parametric modeling enables scalable and robust  
455 detection of spatial expression patterns for large spatial transcriptomic studies. *Genome*  
456 *Biol* **22**: 184.

457 Zhuang X. 2021. Spatially resolved single-cell genomics and transcriptomics by imaging. *Nat*  
458 *Methods* **18**: 18-22.

459